

2023-02

Tissue Artifact Segmentation and Severity Assessment for Automatic Analysis using WSI

HOSSAIN, MD SHAKHAWAT

Independent University, Bangladesh

<https://ar.iub.edu.bd/handle/123456789/581>

Downloaded from IUB Academic Repository

Tissue Artifact Segmentation and Severity Assessment for Automatic Analysis using WSI

MD SHAKHAWAT HOSSAIN^{1,2}, GALIB MUHAMMAD SHAHRIAR³, M M MAHBUBUL SYEED^{1,2}, MOHAMMAD FAISAL UDDIN^{1,2}, MAHADY HASAN^{1,2}, MD SAKIR HOSSAIN³ AND RUBINA BARI⁴

¹RIoT Research Center, Independent University Bangladesh, Dhaka 1229, Bangladesh. (e-mail: mshimul86sets@iub.edu.bd)

²Dept. of Computer Science and Engineering, Independent University Bangladesh, Dhaka 1229, Bangladesh.

³Dept. of Computer Science, American International University-Bangladesh, Dhaka 1229, Bangladesh.

⁴Government Hospital Narayanganj, Dhaka, Bangladesh

Corresponding author: Md Shakhawat Hossain (e-mail: mshimul86sets@iub.edu.bd).

This work was supported in part by the 2022 RIoT Research Grant.

• **ABSTRACT** Traditionally, pathological analysis and diagnosis are performed by manually eyeballing glass-slide specimens under a microscope by an expert. The whole slide image (WSI) is the digital specimen produced from the glass slide. WSI enabled specimens to be observed on a computer screen and led to computational pathology where computer vision and artificial intelligence are utilized for automated analysis and diagnosis. With the current computational advancement, the entire WSI can be analyzed autonomously without human supervision. However, the analysis could fail or lead to wrong diagnosis if the WSI is affected by tissue artifacts such as tissue fold or air bubbles depending on the severity. Existing artifact detection methods rely on experts for severity assessment to eliminate artifact-affected regions from the analysis. This process is time-consuming, exhausting and undermines the goal of automated analysis or removal of artifacts without evaluating their severity, which could result in the loss of diagnostically important data. Therefore, it is necessary to detect artifacts and then assess their severity automatically. In this paper, we propose a system that incorporates severity evaluation with artifact detection utilizing convolutional neural networks (CNN). The proposed system uses DoubleUNet to segment artifacts and an ensemble network of six fine-tuned CNN models to determine severity. This method outperformed current state-of-the-art in accuracy by 9% for artifact segmentation and achieved a strong correlation of 97% with the pathologist's evaluation for severity assessment. The robustness of the system was demonstrated using our proposed heterogeneous dataset and practical usability was ensured by integrating it with an automated analysis system.

• **INDEX TERMS** Tissue artifact, artifact detection, quality evaluation, whole slide image, digital pathology, automated image analysis

I. INTRODUCTION

Conventional pathological image analysis involves examining a biopsy or surgical specimen, fixed on a glass slide using a microscope. This process starts with the biopsy or surgically removing tissue from the body. Then the tissue specimen is processed at different stages to prepare it for analysis and diagnosis. The glass slide tissue preparation involves fixation, dehydration, clearing, paraffin embedding, sectioning, staining and cover-slipping. After that, the glass slide is analyzed under the microscope by an expert pathologist for

the diagnosis. During the examination, the pathologist manually selects and analyzes diagnostically relevant regions by ignoring useless and artifact-affected regions depending on their severity. Inaccurate tissue preparation results in tissue artifacts such as tissue fold, air bubbles, pen marks, dust and tissue tear in the specimen. For example, the tissue fold is produced during the tissue lifting when the tissue adheres to the blade and overlays the normal tissue layer. This is mainly caused by a faulty blade or excessively fatty tissue. The tissue fold contains multiple layers of tissue, it is thicker than the

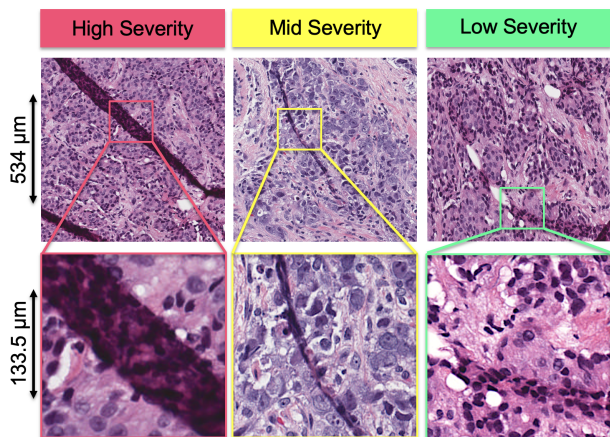


FIGURE 1. Example of artifact severity.

normal regions and shows different characteristics compared to the normal tissue. It can negatively affect the analysis and diagnosis depending on its size, thickness and other properties [1]. The air bubble artifact is produced when the air is trapped under the coverslip due to the thin mounting medium or the tissue section due to the poor flotation bath. Air bubble also changes the histological features of the specimen. Tissue folds and air bubbles are the most common tissue artifacts of tissue-based pathology [2]. Figure 1 shows the example tissue fold and air bubble artifacts with different severity. Ink or pen is used to mark specific regions on a glass slide which sometimes invades the tissue structure making it difficult to assess the area. Dust can also infiltrate the tissue and block the histological features. Tissue tear is the splitting of tissue that is caused by the penetration of faulty forceps [3]. It often breaks the structure of the tissue. Pigment artifacts are caused by the long exposure of tissue to formalin which reacts with the hemoglobin and produces formaldehyde pigments on the tissue. Similarly, color pigment artifacts can be noticed on the CISH specimen caused by the long hybridization time. All these artifacts change original tissue morphology and add irrelevant features which make the analysis challenging [4]. As a result, these artifacts and artifact-affected regions are identified and ignored from the analysis by the pathologists. However, such manual evaluation of artifacts is time-consuming, laborious and subjective to inter- and intra-operator variability. Therefore, the need for an automatic artifact detection method is undeniable, particularly for the digitalization of pathology [5].

In digital pathology, the WSI scanner converts the glass slide specimen into a high-resolution digital image which allows to utilize computer vision and artificial intelligence for analysis and diagnosis. The WSI scanner was approved by FDA in 2017 and since then the WSI-based pathology has been adopted by many laboratories and hospitals for education [6], [7], research [8]–[10] and clinical applications [11]. As shown in Figure 2, modern pathology assembles a digital pathological workflow that is driven by automated sectioning and staining machines for preparing the glass slide

before being converted to a WSI. After that, the WSI is processed using automated image analysis methods and the results of the automatic interpretation are then stored in a central database that is integrated with the laboratory information system. There are several automated image analysis tools that can extract information from the WSI and associate them in ways that a human microscopic examination cannot. The automated analysis of WSI has certainly transcended the ability of pathological analysis to precisely identify the patient’s condition from counting the number of cancer cells, gauging the size of the tumor and predicting the response to treatments.

However, the automated analysis of WSI relies on WSI quality which may be affected by a number of issues. If the WSI quality is subpar, the automated method could produce an inaccurate diagnosis. Scanning artifacts and tissue artifacts are the two main types of artifacts that affect the WSI. The WSI scanner related problems lead to scanning artifacts such as focus blur, noise, low brightness and low contrast. Rescanning the glass slide recovers the WSI from artifacts that were generated due to scanning or hardware problems. In this work, we mainly focused on the tissue artifacts and excluded the scanning or hardware related artifacts as they can be fixed by rescanning the specimen under optimal settings. On the other hand, even if we rescan the glass slide, tissue artifacts like tissue folds or air bubbles that degrade the quality of the glass slide itself cannot be resolved. If the influence of the tissue artifact on the WSI is crucial for the analysis and diagnosis, the artifacts along with the artifact-affected tissue regions must be identified and eliminated from the analysis.

Several methods were proposed previously to identify tissue artifacts, mainly tissue fold or air bubble, utilizing computer vision or machine learning techniques [12]–[22]. However, these techniques don’t consider the influence of artifacts on the analysis and diagnosis to eliminate them. As a result, a significant percentage of the specimen may be excluded from the analysis, which could have been beneficial diagnostically. This is particularly important in molecular analysis, where the presence of biomarkers such as gene and protein are quantified for diagnosis and treatment planning. Existing methods detect tissue artifacts which are then used by the pathologists for the decision to eliminate or include them along with their neighboring regions in the analysis. These methods eliminate a region from analysis if it contains artifacts or part of artifact regardless of their impact on the region. Therefore, it is necessary to evaluate the severity of the tissue artifacts in order to remove them from analysis and diagnosis. Usually in digital pathology, the artifacts are detected automatically and then the decision to eliminate them is taken manually by checking the artifact detection results which makes the system semi-automated.

In this paper, we propose an AI-assisted artifact detection method for a fully automated image analysis system that does not rely on an operator for the decision to eliminate an artifact-affected region from the analysis. The proposed

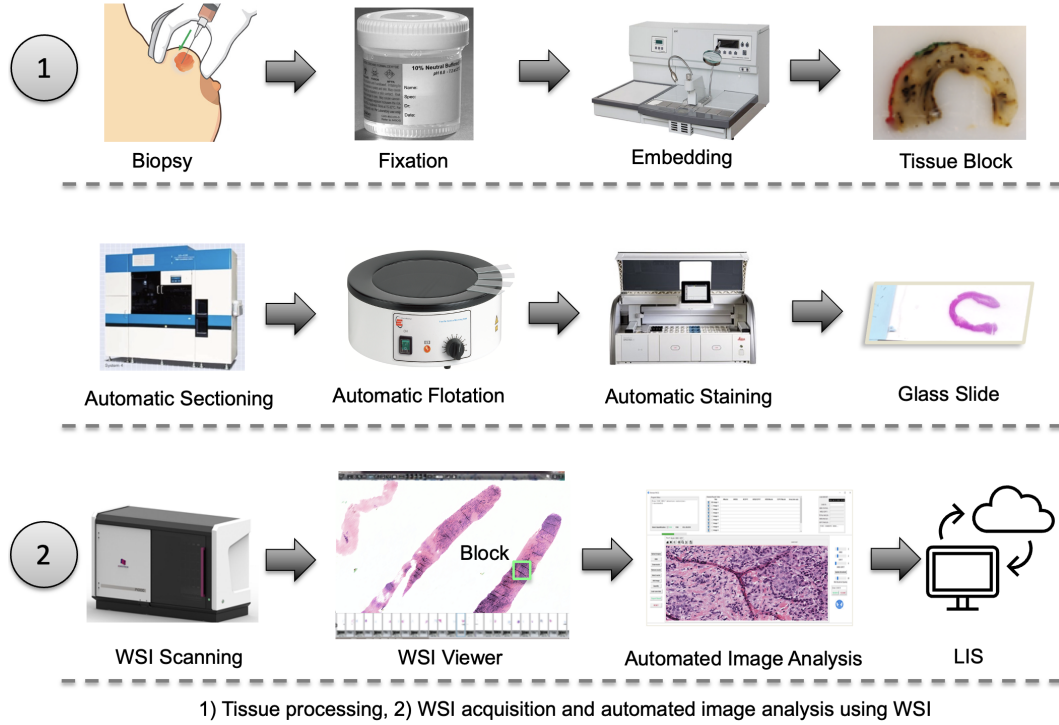


FIGURE 2. Digital pathology workflow for automated image analysis and diagnosis.

system first segments tissue artifacts and then evaluates their severity based on how they affect the analysis, which is then incorporated into the decision to exclude an artifact-affected region from the analysis and diagnosis. For artifact segmentation, multiple U-net-based networks were developed by optimizing the parameters of two well-known U-Net models ResUnet++ and DoubleU-Net. After that, the best network was selected to segment the artifact. U-Net is a CNN that was developed for biomedical image segmentation. Its architecture is based on a fully convolutional network and can achieve precise segmentation when trained with a small number of images. U-net is also computationally fast and a 512x512 image can be segmented in less than a second. To find the best network for determining artifact severity, ten popular CNN-based classification models (i.e., VGG16, VGG19, Xception, ResNet50, InceptionV2, InceptionV3, MobileNet, MobileNetV2, DenseNet121 and NasNetLarge) were fine-tuned by optimizing selective parameters. Then, six suitable networks were combined to form an ensemble network to assess the severity. The proposed system was validated for slides prepared by different laboratories, scanned by multiple scanners and containing different organs and stains. Plus, it can detect the artifact and provide the decision of elimination in less than 10 seconds.

The major contributions of this paper are listed as follows: 1) the development of a fully automated artifact detection method that incorporates severity assessment with the artifact segmentation, 2) the development of a heterogeneous dataset to test the robustness of the artifact detection methods and 3) the evaluation of the proposed method using the heterogeneous

dataset and clinical validation of the system for the practical use.

The rest of the paper is organized as follows, with Section 2 providing a review of the existing literature. The construction of the dataset is described in Section 3 along with an explanation of how the proposed method functions and the experimental protocol. In Section 4, the experiment results are evaluated and in Section 5, the discussion of the study is presented. Section 6 concludes this study and suggests future work.

II. RELATED WORKS

The tissue artifacts detection methods proposed for assisting pathological image analysis can be broadly divided into two categories based on their approach: 1) colorimetric feature-based method and 2) machine learning-based method.

The color distribution based methods [14], [15], [19], [20] utilizes the color properties mainly the saturation-intensity difference of the tissue artifacts to distinguish them from the normal tissue. For example, the tissue folds are thicker compared to the normal tissue areas and absorb more dye. As a result, the tissue fold has a darker appearance than the normal tissue sections, with a higher saturation and lower brightness. This inspired the development of a color-shifting technique to increase the color metric distinction between folded and unfolded regions to detect the folded regions. One of the earliest methods for detecting tissue fold was proposed by Palokangas et al. [19] that utilized the saturation-intensity difference and relied on k-means clustering to identify the folded regions. The choice of cluster number is critical since

a pathological specimen may have various components in a slide, such as nuclei, cytoplasm, background, hazy region, tissue fold or other irregularities. Eventually, this method ended in detecting only the prominent folds and resulted in high false positives in the absence of folds. Practical usability is a major concern for this method as it requires 20X image, takes a long time to process and has only been tested on H&E slides. Bautista et al. [15] proposed another method for detecting tissue fold utilizing its color metric features. This method shifted the saturation by adding an adaptive factor to the RGB values of the pixel depending on saturation and luminance. This shifting enhances a tissue fold pixel more than a normal pixel. After that, a fixed threshold was applied to the change to identify a tissue fold pixel. However, the fixed threshold does not work well for all slides as the color of the WSI varies depending on the scanner, staining protocol of the laboratory and biological variation in slides. For example, a tissue fold in a lightly stained slide that can be similar to a normal region in a highly stained slide. Therefore, this method fails to achieve practical usability. This signifies that a tissue artifact detection method should be demonstrated for multiple scanners and multiple slides prepared by different laboratories to ensure its practical clinical use for digital pathology. Kothari et al. [14] also proposed a different technique for detecting tissue folds based on the saturation-intensity difference, in which folded regions were identified using two adaptive thresholds rather than a single fixed threshold. Based on a connection map that depicts the saturation-intensity differentiation value for different pathological components of the specimen, the thresholds were determined. However, a single colorimetric feature-based approach might not be able to withstand a reproducible image analysis system. Later, the same group presented a different approach [20], combining gray-level texture data with RGB, HSI, CIELUV, and CIELAB features to eliminate tissue folds and pen markings. This method was more robust than the earlier ones when applied to various slides. These methods utilized a low-resolution thumbnail image for quick detection, which is important for practical implementation.

Artifact detection based on only the colorimetric features fails when the staining protocols and scanning profiles change. To overcome this issue, Hossain et al. [12] proposed a machine learning based method that utilizes more intuitive physical properties of the artifacts. They trained support vector machines (SVM) to detect tissue folds and air bubbles from the 1X magnification WSI using the data-driven features obtained from heterogeneous data sets. Babaie et al. [17] proposed a hybrid approach in which they combined the feature extraction capability of CNN with the SVM classifier which needs a small number of data points to classify images. They used DenseNet to extract features and then trained a SVM classifier using the features to detect tissue fold. It achieved an accuracy of 96%. However, the generalized performance was 81% which is significantly low. More importantly, this method relies on 20X magnification

images which is highly time-consuming. Foucart et al. [21] proposed a weakly supervised machine learning method to detect tissue folds from 1.25X images. This method can work when trained with an imprecisely and inaccurately annotated dataset. This is crucial for pathological image analysis as the data annotation is time-consuming and expensive. When used with a GPU-enabled computer, it took about two minutes to segment the tissue fold from a WSI. An open-source tool was developed utilizing the brightness, contrast and other image features for spotting artifacts and evaluating the quality of WSI for automated analysis by Janowczyk et al. [22]. However, this method relies on a 40X image and takes a high time to detect artifacts. For instance, in a demonstration to evaluate 450 image blocks, this method took 135 minutes in a computer with four hyperthreaded core processors. Thus, it is not suitable for routine clinical use.

None of the above mentioned methods except the Janowczyk et al. [22] considered the severity of the artifact for eliminating them from the analysis. However, this is crucial for developing a fully automatic image analysis and diagnosis system. Moreover, the detection should be robust and fast to ensure its practical use. In this paper, we proposed an efficient and practically reliable method that not only segments the artifacts but also assesses their severity to incorporate it for the decision to eliminate or include them in the analysis.

III. MATERIALS AND METHOD

A. DATASET

For this study, we developed a heterogeneous dataset with specimens from multiple labs that were scanned using different scanners and contained a variety of organs and stains. The specimens used for the test were entirely different from those used for training and validating the networks, as shown in Figure 3. This was done to ensure the robustness of the proposed method.

For the artifact segmentation experiment 960 image blocks were extracted from 26 WSIs at 1x which included 480 tissue fold images and 480 air bubble images. Among the 26 slides, 20 were scanned using 3DHISTECH Panoramic Desk Scanner and 6 were scanned using HAMAMATSU NanoZoomer scanner. The 26 slides were produced from human biopsy and included major tissue organs such as brain, liver, lung, stomach, intestine, spleen, and heart. The staining included H&E, IHC-p40, IHC-B-catenin, IHC-CD34, IHC-CD3, Masson's trichrome, PAS (Periodic acid Schiff), Azan trichrome and CISH (chromogenic in situ hybridization). The biopsy glass slides were produced in two different laboratories. These artifact-affected images were annotated by three sub-specialized breast pathologists to generate mask for artifact segmentation experiments. These images contain artifacts of different severity which were identified manually by the experts as high, mid and low for training and validating the severity assessment classifier. The 960 images included 320 images of each severity.

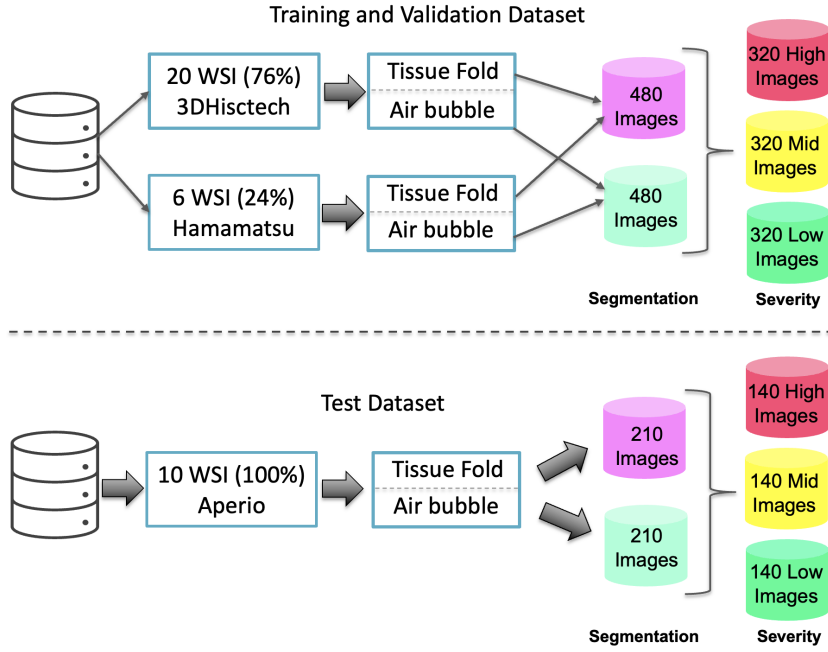


FIGURE 3. Heterogeneous data distribution.

A set of another 420 artifact-affected images were extracted from 10 WSIs at 1x which were scanned by Aperio scanner. These images were produced from a completely different slides, prepared and scanned by a different laboratory at Sunnybrook Health Sciences Centre, Toronto, Ontario, Canada [23]. The 420 images contained 210 tissue fold and 210 air bubble images which were used for testing the artifact segmentation networks. Then, these images were assessed independently by three experts to determine their severity. It includes 140 high, 140 mid and 140 low severity images which were used to test the severity assessment classifier. Table 1 shows the distribution of data for training, validating and testing the segmentation and severity assessment networks. As the dataset contains human specimens, we obtained ethical approval for this study from the Institutional Review Board of Independent University, Bangladesh (approval code: 2022-SETS-002).

TABLE 1. Training, validation and test data distribution for segmentation and severity assessment experiment.

| | Segmentation | | Severity | | |
|------------|--------------|------------|----------|-----|-----|
| | Tissue fold | Air bubble | High | Mid | Low |
| Training | 384 | 384 | 256 | 256 | 256 |
| Validation | 96 | 96 | 64 | 64 | 64 |
| Test | 210 | 210 | 140 | 140 | 140 |

B. ARCHITECTURE OF THE PROPOSED SYSTEM

The proposed method utilizes low magnification WSI such as 1X to segment artifacts and estimate their severity for the decision to eliminate them from the analysis. The WSI is very large such as $100,000 \times 100,000$ pixels and stored using

a multi-resolution pyramid architecture. The early layers of the pyramid provide low-resolution images, while deeper layers provide higher resolution. Processing the WSI image is a time-consuming task because of its massive size and diversity. High-resolution WSI such as 20X-60X is used for tasks that require finer details, such as identifying tissue structures, recognizing bio-marker signals, and detecting focus error. High-resolution image blocks take a long time to process. On the other hand, low-resolution WSI, such as 1X-5X contains coarse information and can be processed faster. The proposed method utilized the 1X magnification WSI for rapid evaluation yet achieved adequate precision for reliable artifact detection. Figure 4 shows the architecture of the proposed system that has mainly three phases: 1) Scanning the WSI and diving it into blocks, 2) pre-processing the blocks and 3) artifacts segmentation, severity assessment of artifact segmented blocks and visualization for the user.

Algorithm 1 explains the proposed system which starts with dividing the WSI into non-overlapped and fixed-size image blocks of 200×200 pixels. Then for each block, *WhiteScore* is estimated. An image block containing mostly white pixels was excluded for artifact checking. A pixel is considered white if its intensity is higher than 200. The *WhiteScore* is the percentage of white pixels in a block. We excluded a block if it contains more than 75% white pixels. Otherwise, it is converted to the sRGB color space. Then, two different DoubleU-Net models are applied on the block: one for tissue fold segmentation and the other for air bubble segmentation. The U-Net models were trained for segmenting the particular artifacts from the block. If the block contains any of the artifacts it is then assessed using the severity assessment classifier to estimate the influence of

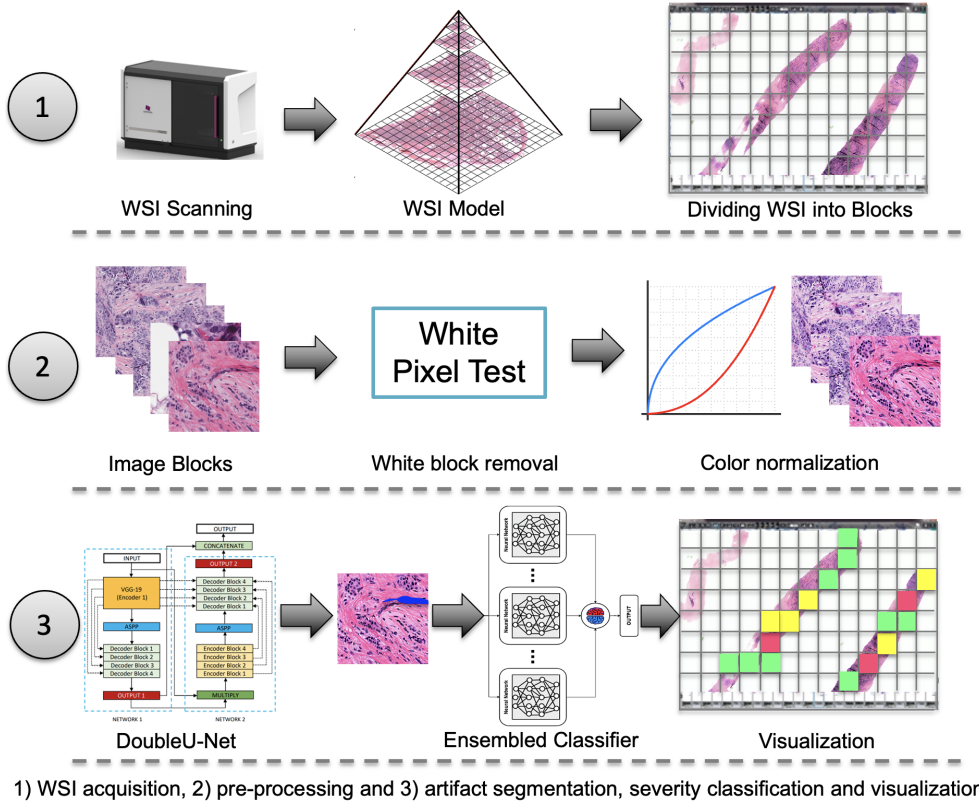


FIGURE 4. Architecture of the proposed system.

the artifact on the block. The severity classifier classifies the influence as High, Mid or Low. Finally, this information is utilized for visualizing the artifacts along with their severity in the WSI viewer for user interpretation.

In this study, the existing CNN models and technology were utilized to find the best networks for the proposed work. We constructed a unique heterogeneous dataset for training, validation and testing the networks for this purpose. Then a set of 480 segmentation networks and 720 severity classification networks were created by modifying selected hyper-parameters of existing popular networks that had already been established for related works and fine-tuned using the heterogeneous dataset. The best networks were then found from the candidates using an exhaustive grid search. The details of tissue artifact segmentation and severity assessment method are explained in the following sections.

1) Tissue Artifact Segmentation

We have detected tissue fold and air bubble artifacts which are the most common artifacts found in histopathology slides. However, we plan to include other artifacts such as dust and pen marks in future. We have trained two separate DoubleU-Net [24] model for detecting tissue fold and air bubble from 256X256 image blocks extracted from 1X WSI. Traditionally, U-net [25] uses an encoder-decoder-based approach to accomplish semantic segmentation, where each pixel of the image corresponds to a class. DoubleU-Net [24] architecture

uses two U-nets in a sequence with two encoders and two decoders to capture more semantic information efficiently, an advancement over the conventional U-Net. It also uses Atrous Spatial Pyramid Pooling (ASPP) to extract high-resolution feature maps that lead to superior performance. The first U-Net uses a pre-trained VGG-19 [26] as the encoder followed by a decoder sub-network. The VGG-19 network is trained on the ImageNet dataset. In the DoubleU-Net architecture, an input image is first fed to the VGG-19 encoder based U-Net which produces the predicted masks for the input. Then, the original input and its masks are multiplied to feed the second U-net network which produces another mask. After that, the masks of both U-Nets are concatenated to get the final predicted mask which serves as the output of the DoubleU-Net network.

We annotated the input images to create binary masks for training the network. The image dataset contains 480 tissue fold and 480 air bubble images which were annotated manually for training the U-net network. The tissue fold segmentation networks were trained and validated using 80% and 20% of the 480 images, accordingly. The air bubble segmentation networks were trained, validated and tested similarly using the air bubble images. Data was augmented by applying vertical flip, horizontal flip and rotating at 15 degrees for the training. We have experimented with ResUnet++ and DoubleU-Net using different optimizers, loss functions and learning rates for both tissue fold and air

bubble segmentation. Both the tissue fold and air bubble segmentation network achieved the best performance for DoubleU-Net when trained by an RMSprop optimizer with Dice Coefficient loss function and Sigmoid output function. The epoch was 100 and the learning rate was 0.0001.

Algorithm 1 Artifact segmentation and severity classification

```

1: Input:  $I_{WSI}, W_{th}, SegNet_{TF}, SegNet_{AB}, M, P, G, f$ 
    $I_{WSI}$ : the 1X WSI
    $W_{th}$ : threshold to eliminate white blocks
    $SegNet_{TF}$ : Trained DoubleU-net for tissue fold
    $SegNet_{AB}$ : Trained DoubleU-net for air bubble
    $G$ : base models with parameters
2: Initialisation:
    $G = \{g_1, g_2, g_3, \dots, g_n\}$ ,
3:  $I_{block} = \text{Divide } I_{WSI} \text{ into } 200 \times 200 \text{ pixels blocks}$ 
4: while  $I_{Block} \neq NIL$  do
5:    $WhiteScore_I = \text{Percent of white pixels in } I_{Block}$ 
6:   if  $WhiteScore_I \leq W_{th}$  then
7:     if  $C_{Linear} \leq 0.0031$  then
8:        $I_{sRGB} = 12.92 \times C_{Linear}$ 
9:     else
10:       $I_{sRGB} = 1.0552 \times C_{Linear}^{\frac{1}{2.4}}$ 
11:    end if
12:    Apply  $SegNet_{TF}$  on  $I_{sRGB}$ 
13:     $I_{TF} = \text{Tissue fold affected blocks}$ 
14:    Apply  $SegNet_{AB}$  on  $I_{sRGB}$ 
15:     $I_{AB} = \text{Air bubble affected blocks}$ 
16:    if  $I_{TF} \neq NIL$  or  $I_{AB} \neq NIL$  then
17:      while  $i \leq n$  do
18:         $G_i \leftarrow \text{Load base models}$ 
19:         $f_i = G_i(I_{ROI})$ 
20:         $i = i + 1$ 
21:      end while
22:      Load meta model with the  $n + 1$  parameters
         $\{\alpha, \beta, \gamma, \eta, \dots, \lambda\}$ 
23:       $y = \alpha + \beta f_1 + \gamma f_2 + \delta f_3 + \eta f_4 + \dots + \lambda f_n$ 
24:       $MAX = \text{maximum}(y)$ 
25:      if  $y(1) == MAX$  then
26:         $\psi \leftarrow \text{High}$ 
27:      else if  $y(2) == MAX$  then
28:         $\psi \leftarrow \text{Mid}$ 
29:      else
30:         $\psi \leftarrow \text{Low}$ 
31:      end if
32:    end if
33:  end if
34: end while
35: return  $\psi$ 

```

2) Artifact Severity Assessment

The artifact segmentation is followed by a severity assessment to determine if the artifact and neighboring affected regions should be excluded from the diagnosis. We classified

the severity of the artifacts as High, Medium, and Low, resulting in multi-class classification. As illustrated in Figure 5, we used ensemble learning for severity classification. Ensemble architecture incorporates the strengths of multiple models while mitigating their weaknesses, resulting in higher accuracy than individual models [27], [28].

In an ensemble architecture, multiple models are integrated in layers. In the first layer, multiple models are trained individually using the input images to predict the output classes. The models of the first layer are called base models or classifiers. The outputs of the base layers serve as the input to the model of the second layer, known as the meta-model. The output class is predicted by the meta-model utilizing the outputs of the base models as features. The proposed system employs a single ensembled architecture to predict the severity of artifacts for both tissue folds and air bubbles. At first, we trained ten candidate CNN classifiers individually which are VGG16, VGG19, Xception, ResNet50, InceptionV2, InceptionV3, MobileNet, MobileNetV2, DenseNet121 and NasNetLarge to predict the severity of artifacts regardless its type. The candidates were pre-trained using the ImageNet dataset. To determine the best network architectures, we investigated the performance of the candidate models for various optimizers, loss functions and other parameters. After that, the top six networks were selected as base models to form the ensemble architecture. The best six networks were then selected as the base models of the ensemble architecture. In the ensemble architecture, the outputs of the six base classifiers were fed to a different meta-model. We have experimented with ten different candidates which include Logistic Regression (LR), K-nearest neighbor (KNN), Decision Tree (DT), Random Forest (RF), AdaBoost Classifier (Ada), Xtreme Gradient Boosting Classifier (XGB), Gradient (GB) Boosting Classifier, Gradient Boosting (GB) Regression and Gaussian Naive Bayes (GNB) for meta models. LR, KNN and SVM achieved the best performance in the experiment, however, we recommend using LR as it achieved the highest accuracy for all combinations of base networks.

We used a dataset of 960 images of tissue fold and air bubble artifacts which included 320 images for each category High, Mid and Low for training and validating the ensemble model. A separate dataset of 420 images which included 140 images for each category was used to test the ensemble model. This was done to ensure that the proposed method is tested using a completely unseen dataset.

IV. RESULTS

We have evaluated the artifact segmentation results of segmentation networks in terms of IoU, accuracy, AUC and precision. The IoU is the number of pixels common between the annotation mask in the ground truth and the segmentation mask by the proposed method divided by the total number of pixels covered by both for an image block, as given in Eq. (1). The sum of the IoU scores for various images divided by the total number of images is then used to determine the average IoU for a network. An artifact-affected image is termed true

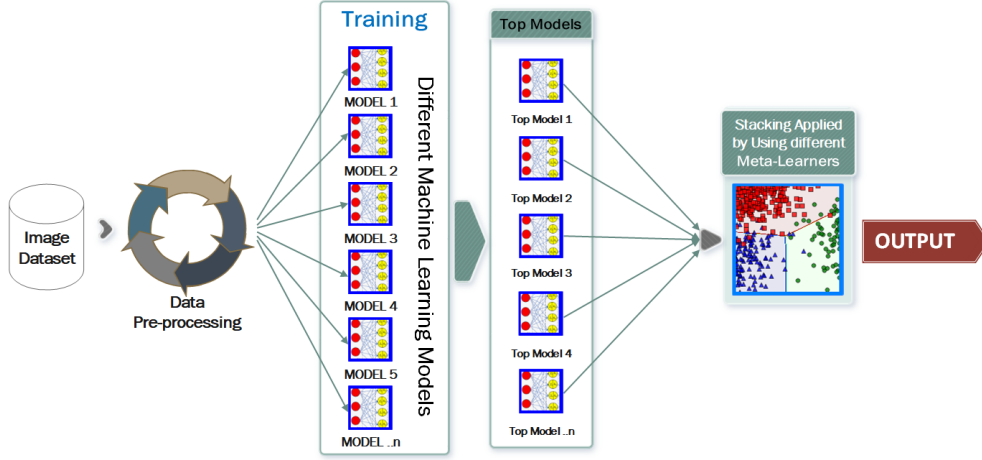


FIGURE 5. Proposed ensemble approach for artifact severity assessment.

positive if the IoU score exceeds a predetermined threshold; otherwise, it is considered a false negative. An artifact-free image is a true negative if the IoU score is less than the threshold; otherwise, it is considered a false positive. Then, using Eq. (2) and Eq. (3), the accuracy and precision value of the network are determined. The accuracy values obtained by changing the predetermined threshold value are used to estimate AUC.

$$IoU = \frac{Annotation \cap Segmentation}{Annotation \cup Segmentation} \quad (1)$$

$$Accuracy = \frac{True\ Negatives + True\ Positives}{All\ Samples} \quad (2)$$

$$Precision = \frac{True\ Positives}{True\ Positives + False\ Positives} \quad (3)$$

In the severity assessment experiment, the accuracy on test data was used to select the base models among the candidates. Further, the confusion matrices as well as the micro- and macro-averaged AUC of ROC curves were shown. The key difference between macro and micro averaging is that the former assigns equal weight to each class whereas the latter does so for each sample. If the number of samples for each class is the same both macro and micro will provide the same score. The severity assessment ensemble model was then evaluated using a confusion matrix, which is a widely recommended method for evaluating multi-class classification problems. But we relied on its statistical correlation with experts' manual judgement to guarantee the validity. Both the Pearson and Spearman rank correlations were used to estimate the correlation.

A. EVALUATION OF ARTIFACT SEGMENTATION

We have trained two different networks to segment tissue folds and air bubbles. To find the best networks, we have experimented with ResUnet++ and DoubleU-Net models. The

models were trained for the various hyperparameters listed in Table 2 which produced 480 candidate networks. Based on their accuracy, average IoU, AUC and precision on the test data, the best networks were selected for segmenting each type of artifact. The most effective segmentation of tissue folds and air bubbles was accomplished using DoubleU-Net networks with RMSpropos optimizer, Dice Coefficient loss function, and learning rate 0.001. As the candidates were being trained and validated, we calculated their accuracy, precision, loss and IoU curve as well. Figure 6 shows the training and validation IoU for the best networks based on ResUnet++ and DoubleU-Net models to segment both tissue folds and air bubbles. The performance evaluation of the best ResUnet++ and DoubleU-Net networks for segmenting tissue folds and air bubbles on the test dataset is illustrated in Figure 7. From Figure 6 and 7, it can be seen that the DoubleU-Net based networks outperformed the ResUnet++ on both occasions. Therefore, the DoubleU-Net based networks, $SegNet_{TF}$ and $SegNet_{AB}$ were selected to segment the tissue fold and air bubble artifacts, respectively. The $SegNet_{TF}$ achieved an average test IoU of 98.02% for 95% threshold, test accuracy of 98.33% for 90% IoU threshold and test accuracy of 100% for 85% IoU threshold. Similarly, the $SegNet_{AB}$ network had an average test IoU of 99.11%, test accuracy of 100% for 90% IoU threshold and test accuracy of 100% for 85% IoU threshold. Figure 8 shows the result of tissue fold and air bubble segmentation using selected segmentation networks. The proposed method achieved 99.33% and 99.11% accuracy using a 90% IoU threshold for segmenting tissue fold and air bubble artifacts from 1X WSI, respectively. We have also compared the proposed method's artifact segmentation result with the previous methods, as shown in Table 3. The results show that the proposed method achieved the highest accuracy among the artifact detection methods when implemented on the same heterogeneous dataset. Furthermore, this method makes use of 1X magnification images, which is crucial for practical use. Using high magnification images, such as 10X

TABLE 2. Optimization of hyperparameters for ResUnet++ and DoubleU-Net to find the best segmentation networks for tissue fold and air bubble.

| Criteria | Search Space |
|--------------------|------------------------------|
| Pre-trained Models | [ResUnet++, DoubleU-Net] |
| Epoch | [25, 50, 100, 150, 200] |
| Batch size | [8, 16, 32] |
| Learning rate | [0.0001, 0.001, 0.01, 0.03] |
| Optimizer | [Adam, Adamax, RMSprop, SGD] |
| Loss function | [Dice Coefficient Loss] |

or higher, prolongs the artifact segmentation process, making it unsuitable for practical use.

B. EVALUATION OF SEVERITY ASSESSMENT

We trained the ensemble model to assess the severity of artifact-affected regions as high-severity, mid-severity and low-severity regardless of the type of tissue artifacts. In order to find the best networks for the base model, we have investigated the performance of ten CNN models for different batch sizes, learning rates, optimizers and loss functions, as shown in Table 4. This generated a search space of 720 candidate networks to train and select the best networks as base models. For training, we have adopted the transfer learning approach and utilized the pre-trained models using the ImageNet dataset. In transfer learning, we freeze the convolution base of the models and trained only the dense layers using the training and validation dataset. 80% of the images were used for training and 20% were used for validating the models.

Based on the test accuracy of the candidate networks, we selected 6 networks as the base models, as shown in Table 5. Figure 9 shows the training and validation accuracy and loss curves of the selected base networks. The confusion matrices and the receiver operating characteristics curves for the selected based models are shown in Figure 10 and Figure 11, respectively. The results of these experiments show that the CNN-based models achieve good accuracy in assessing the severity of artifacts in the validation and test dataset. However, in order to ensure the generalized performance of the proposed system, we have combined the multiple base models which were trained separately to form an ensemble architecture. Multiple research showed that ensemble architecture achieves higher generalization capabilities compared to an individual model for classification task [29].

Then, the base networks are stacked where each network predicted the severity of a given input image, which were then utilized as a feature to train a meta-classifier to predict the final outcome. We employed different combinations of selected base networks with different meta-classifiers and compared their results to determine the best ensemble architecture. In the network comparison (as shown in Table 6), the logistic regression outperformed the other meta-classifiers when applied with the network combinations. As a result, we have chosen and suggested an ensemble architecture for the proposed system by stacking the top six networks as base models and the logistic regression as the meta-classifier.

The proposed method achieved a classification accuracy of 99.99% for evaluating the severity of artifact-affected regions.

We have also evaluated the performance of the proposed method subjectively in which the severity assessment results were compared with the pathologist’s manual scores. The Spearman’s rank correlation was 0.99 and the Pearson correlation was 0.97 ($p < 0.001$) for 418 degrees of freedom which indicate a high concordance between the pathologist’s manual observation and the proposed method. Figure 12 shows the comparison between the proposed method and the pathologist’s manual evaluation of severity assessment. For this evaluation, we have used another set of test images which contained 420 images unseen to the network. Pathologists scored 140 image blocks as high severity, 140 as medium severity, and 140 as low severity out of 420 images. The proposed method classified 129 blocks as high, 153 as mid, and 139 as low severity. Thus, the proposed method incorrectly classified 13 blocks as mid severity whereas pathologists rated them as high severity. This is particularly important in molecular analysis, where the presence of biomarkers such as gene and protein are quantified for diagnosis and treatment planning.

C. EVALUATION FOR PRACTICAL USE

The assessment of the proposed method for routine clinical application is crucial to ensure its practical use in the hospital and pathology laboratories. In medical research, it is necessary to incorporate the feedback of practitioners to validate a system for clinical use. In this work, we did the same with three expert pathologists to identify the key system considerations for the clinical deployment and then assess the fitness of the proposed system against them. The identified key system considerations are the generalized performance with heterogeneous datasets, time of execution, and integration with the application for pragmatic use.

The state-of-the-art methods were trained and tested using specimens prepared by the same laboratory. As a result, these methods failed when applied to the specimens provided by different labs or contains different organs or stains. To ensure the generalized performance of the proposed method, we therefore, prepared a heterogeneous dataset that contains specimens of different stains and organs. Alongside, these specimens were prepared by different laboratories and were scanned by different scanners. When tested with this dataset, the proposed method achieved an accuracy of over 99%, which conclusively confirms the generalized usability of the method.

The time of execution is another key consideration as the processing time increases exponentially with larger WSI images (e.g., WSI image at 10X~40X magnification). Therefore, the proposed method utilized 1X magnification image for artifact detection and severity assessment. This selection significantly reduced the execution time. For example, when applied on 5 WSIs using a MacBook with an Apple M1 chip and a 8-core CPU, the proposed method took time in between

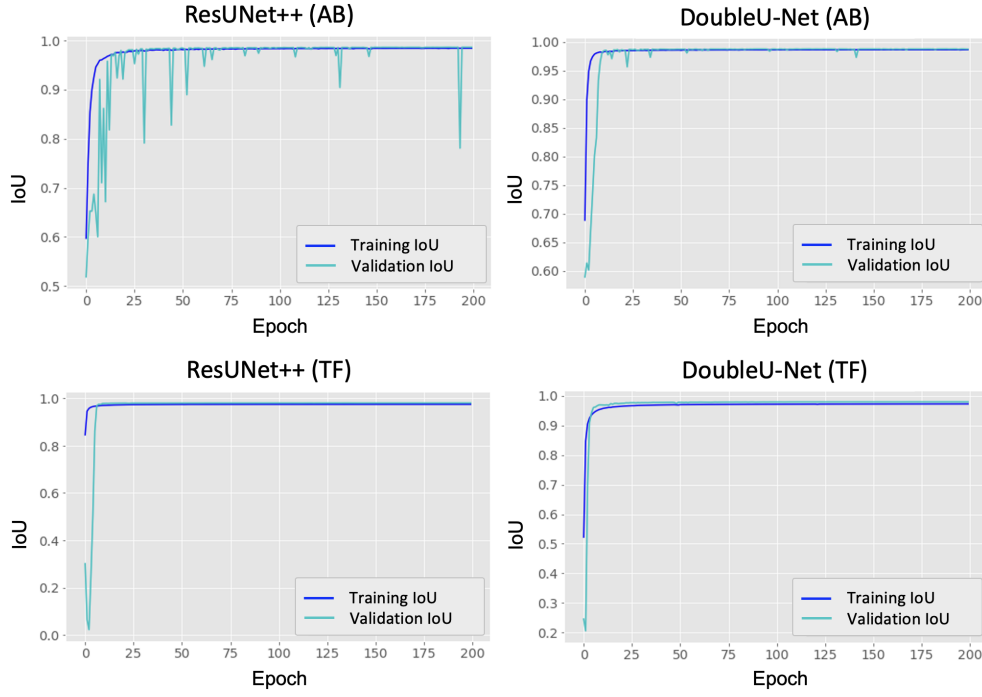


FIGURE 6. Training and validation IoU of best networks of ResUNet++ and DoubleU-Net for tissue fold (TF) and air bubble (AB) segmentation.

TABLE 3. Comparison of artifact segmentation methods.

| Method | Artifacts | Magnification | Average accuracy on homogeneous dataset | Average accuracy on heterogenous dataset |
|------------------------|------------------------------------|---------------|---|--|
| Palokangas et al. [19] | Tissue fold | 20X | 85.46% | - |
| Bautista et al. [15] | Tissue fold | 1X | 77.91% | - |
| Kothari et al. [14] | Tissue fold | 1X | 77% | - |
| Foucart et al. [21] | Tissue fold | 1.25X | 91% | - |
| Babaie et al. [17] | Tissue fold | 20X | 81% | - |
| Janowczyk et al. [22] | Tissue fold, ink mark & air bubble | 40X | 95% | - |
| Hossain et al. [12] | Tissue fold & air bubble | 1X | 97.7% | 90% |
| Proposed | Tissue fold & air bubble | 1X | 99% | 99% |

-, Not available.

TABLE 4. Optimization of hyperparameters for 10 different models to select base models for severity classification.

| Criteria | Search Space |
|--------------------|--|
| Pre-trained Models | [VGG16, VGG19, Xception, ResNet50, InceptionV2, InceptionV3, MobileNet, MobileNetV2, DenseNet121 and NasNetLarge] |
| Epoch | [25, 50, 100] |
| Batch size | [8, 16, 32] |
| Learning rate | [0.0001, 0.001, 0.01, 0.03] |
| Optimizer | [Adam, Adamax, RMSprop] |
| Loss function | [Categorical cross entropy, Kullback Leibler Divergence] |

5 and 13 seconds. This time is slightly higher than the SVM based method proposed by Hossain et al. [12]. However, our method incorporated the severity assessment with the artifact segmentation that is missing in the earlier work. Nonetheless, the execution time is still efficient enough for practical use considering the fact that the contemporary WSI scanners take approximately 1 to 2 minutes only to scan an entire WSI.

The last consideration is to integrate the method with automated image analysis tools for pragmatic use. To date, most of the image analysis techniques are created as standalone applications or as WSI viewer plug-ins. In this work, we developed an application using python and integrated it with an image analysis application which is automatic HER2 quantification. This system uses H&E specimens to identify and select representative invasive breast cancer regions which are then copied to the CISH WSI using image registration for further quantification. For accurate HER2 quantification, which the artifacts may impair, the selection of invasive regions is essential. In addition, eliminating a low severity artifact affected block may have an effect on the region selection process for HER2 measurement. In order to segment the artifacts, and show their severity using different colors along with the severity score, we created an application for the proposed method using Python’s Tkinter library. The feedback from the pathologists was considered in making the application simple to use. A 3 scale Likert with options *good*,

TABLE 5. Selected neural networks as the base model for ensemble learning.

| Network | Pre-trained Model | Optimizer | Loss Function | Validation Loss | Test Accuracy |
|-----------|-------------------|-----------|---------------|-----------------|---------------|
| Network 1 | XCEPTION | RMSprop | CCE | 0.0103 | 0.9976 |
| Network 2 | MobileNet | RMSprop | KLD | 0.0092 | 0.9976 |
| Network 3 | MobileNetV2 | RMSprop | CCE | 0.0024 | 0.9970 |
| Network 4 | DenseNet121 | RMSprop | CCE | 0.0034 | 0.9970 |
| Network 5 | MobileNetV2 | RMSprop | KLD | 0.0206 | 0.9966 |
| Network 6 | VGG19 | RMSprop | CCE | 0.0216 | 0.9916 |

CCE, Categorical Cross Entropy; KLD, Kullback Leibler Divergence.

TABLE 6. Test accuracy comparison for different meta models.

| Meta Models | LR | KNN | SVM | DT | RF | Ada | XGB | GBR | GBC | GNB |
|----------------|-------|-------|-------|-------|-------|-------|-------|-------|-------|-------|
| Top 2 Networks | 99.99 | 99.99 | 99.82 | 99.64 | 99.64 | 99.99 | 99.99 | 99.99 | 99.99 | 99.82 |
| Top 3 Networks | 99.99 | 99.82 | 99.99 | 99.64 | 99.64 | 99.99 | 99.99 | 99.99 | 99.99 | 99.82 |
| Top 4 Networks | 99.99 | 99.99 | 99.99 | 99.81 | 99.82 | 99.99 | 99.82 | 99.82 | 99.99 | 99.99 |
| Top 5 Networks | 99.99 | 99.99 | 99.99 | 99.81 | 99.82 | 99.99 | 99.82 | 99.99 | 99.82 | 99.99 |
| Top 6 Networks | 99.99 | 99.99 | 99.99 | 99.90 | 99.99 | 99.96 | 99.99 | 99.82 | 99.82 | 99.99 |

LR, Logistic Regression; KNN, K-Nearest Neighbors; SVM, Support Vector Machine; DT, Decision Tree; RF, Random Forest; Ada, AdaBoost Classifier; XGB, Extreme Gradient Boosting Classifier; GBR, Gradient Boosting Regression; GBC, Gradient Boosting Classifier; GNB, Gaussian Naive Bayes Classifier.

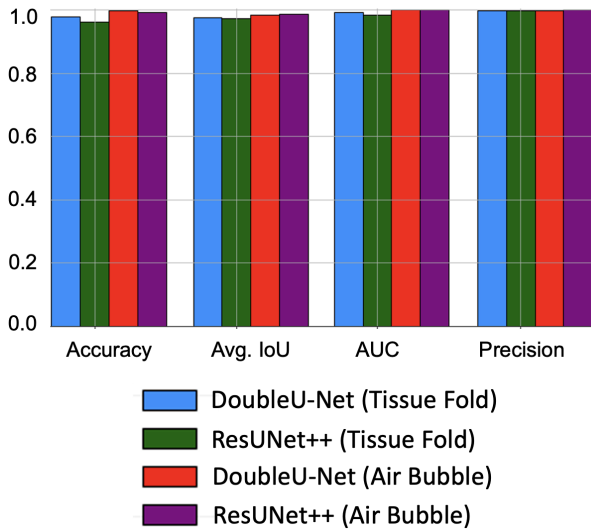


FIGURE 7. Comparison of best networks of ResUNet++ and DoubleU-Net for segmenting tissue folds and air bubbles from test dataset.

average and poor was included in the application to rate its performance by the pathologists.

V. DISCUSSION

In this paper, we have proposed a method that segments tissue artifacts from WSI and assesses their severity to guide the decision to eliminate them from analysis and diagnosis. Existing methods are impractical in this regard, as they often eliminate a region if it is overlapped by the artifact regardless of its size and impact on further analysis. This could result in the loss of significant regions and lead to inaccurate analysis. The proposed method incorporated the severity assessment of artifact affected regions with the artifact segmentation for precise automated analysis. This type of system is crucial for developing a fully automated image analysis system for digital and computational pathology. The proposed method

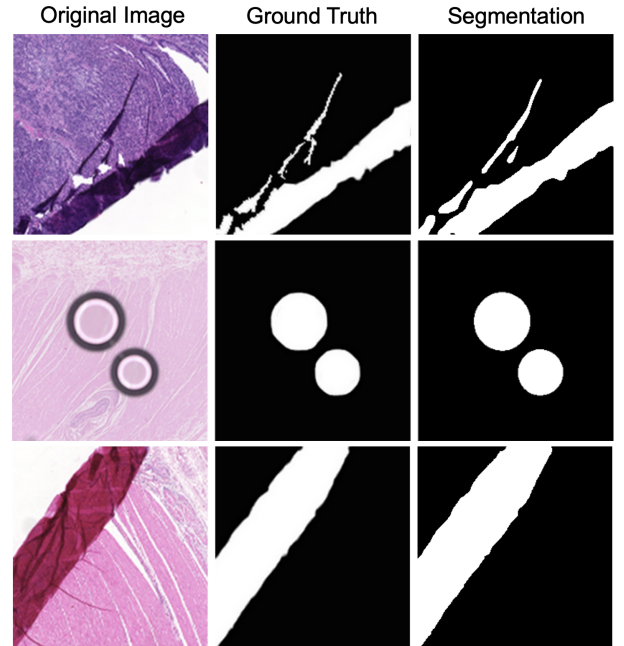


FIGURE 8. Artifact segmentation result by proposed networks.

was also found more accurate in segmenting artifacts than the earlier methods when compared on the same dataset. The robustness and practical usability of the method was confirmed through objective and subjective evaluations. In general, Medical imaging systems are evaluated based on objective metrics only, and therefore, either fail to offer a practical implementation or fall short of achieving the desired performance. Therefore, a subjective evaluation of the proposed method and the system were carried out to ensure its pragmatic use.

In pathology, the color and texture of the tissue specimen vary a lot depending on the stain, organ and tissue type. Previously proposed methods were trained with a homogeneous

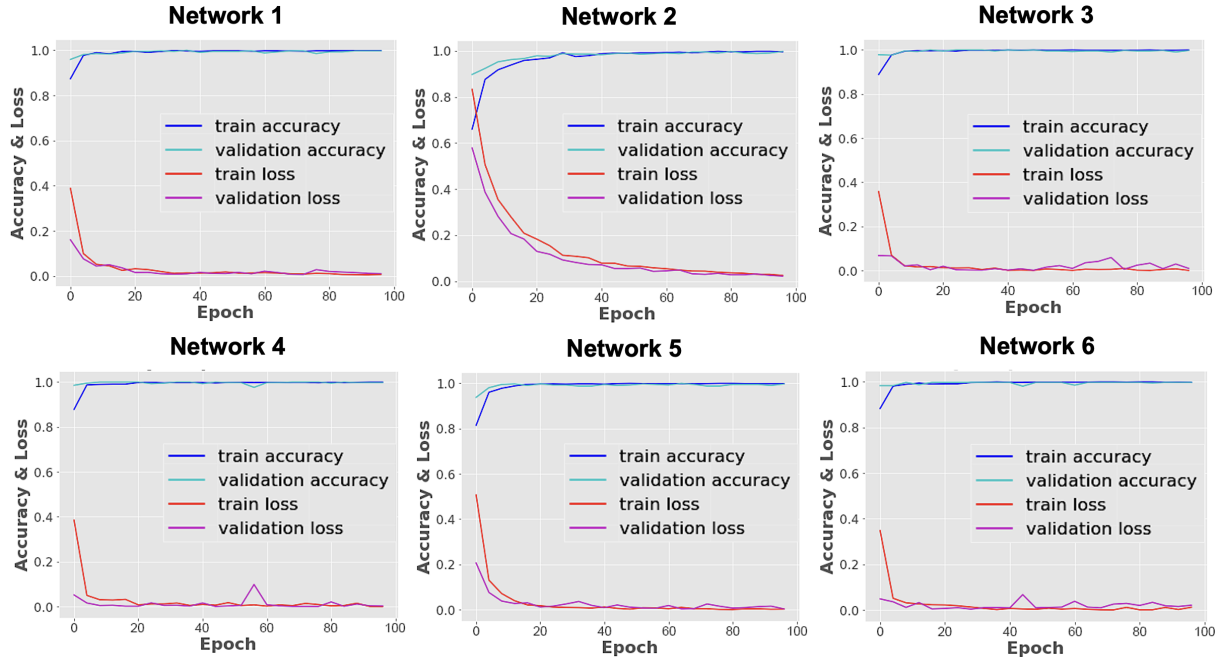


FIGURE 9. Selected Neural networks.

dataset and thus failed to achieve generalized performance when applied to the specimen prepared under different conditions. Therefore, we prepared a heterogeneous dataset that contains specimens prepared by different laboratories having different staining and organs, and the WSIs were scanned by different scanners. The proposed method was validated on this dataset to ensure generalization ability. The results were then evaluated based on multiple objective metrics, such as accuracy, IoU, AUC and precision. We also evaluated the results based on the pathologists' scores in which the proposed method achieved high concordance. This type of subjective evaluation is really useful to ensure the routine application of the system in hospitals and pathology laboratories.

Additionally, the practical usability of the proposed method was evaluated for routine clinical use based on the feedback of pathologists and technicians. The proposed method also achieved the practical requirement of time by utilizing the low magnification WSI such as 1X WSI for segmentation and severity assessment in contrast with the Janowczyk et al. method [22] that relies on 40X image.

However, the proposed artifact detection method can unexpectedly detect artifact-free regions as false positives. The severity evaluation method should then classify the false positives as low severity in order to deal with it. However, such experiments were not included in this study. Another limitation is that the effect of image magnification on the severity assessment result was not studied and the experiment only used 1X magnification images. However, the proposed method achieved a satisfactory accuracy of 97%.

VI. CONCLUSION

In this paper, we proposed a practical artifact detection method by incorporating artifact segmentation and severity assessment for an autonomous image analysis system for digital and computational pathology. In addition, a heterogeneous dataset was prepared for evaluating the artifact detection method. The proposed system was found robust in the demonstration using the heterogeneous dataset. The proposed method achieved approximately 99% accuracy for artifact segmentation which is higher than any previous methods. Plus, it determined the severity of artifacts with 97% accuracy which was not considered in the earlier methods. The result of our severity assessment experiment suggests that the ensemble architecture achieves more stable classification performance compared to the individually trained models when tested on a heterogeneous dataset. In the artifact segmentation experiments, the DoubleU-Net model was found more accurate than the ResUnet++ for different parameters. The practical usability of the system was also evaluated by integrating it with the pathology workflow. Then, the system was validated for routine clinical application using both objective and subjective approaches.

In the future, the detection of pen marks, tissue dust and other artifacts can be included. The application of non-CNN models such as vision transformers can be evaluated for the proposed work. The development of a WSI plug-in to integrate the proposed method with the WSI viewer is another future work.

REFERENCES

- [1] Bindhu, P., Krishnapillai, R., Thomas, P. & Jayanthi, P. Facts in artifacts. *Journal Of Oral And Maxillofacial Pathology: JOMFP*. 17, 397 (2013)

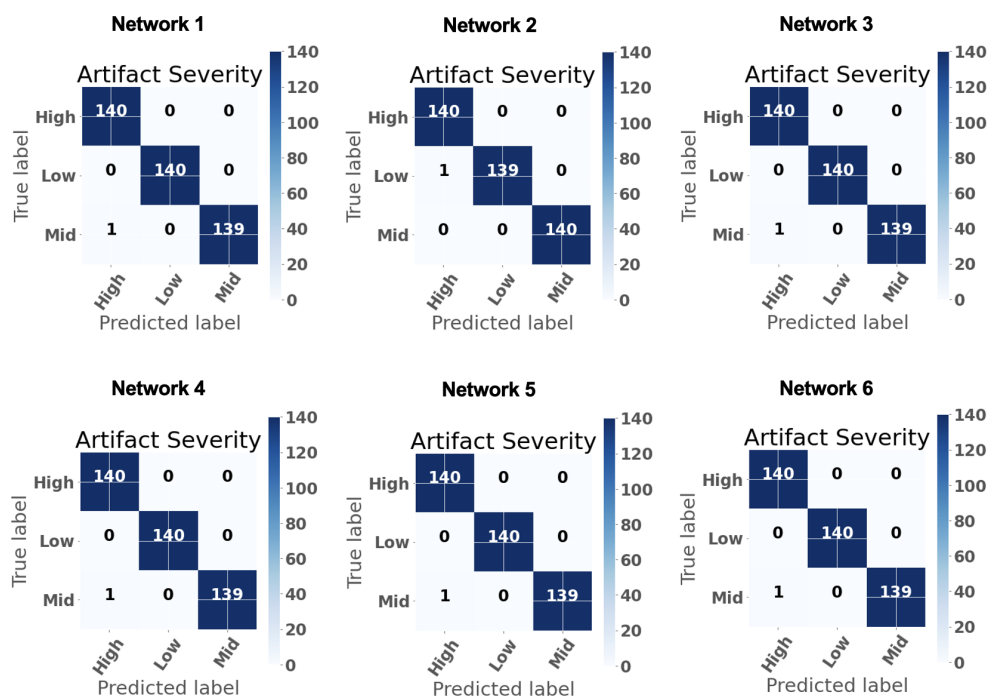


FIGURE 10. Confusion matrices of the selected networks for validation dataset.

- [2] Ekundina, V. & Eze, G. Common artifacts and remedies in histopathology (a review). *African Journal Of Cellular Pathology*. pp. 1-7 (2015)
- [3] LB, T. & Zaki, S. A review of artifacts in histopathology *J. Oral Maxillof. Pathol.* **22**, 279 (2018)
- [4] Wright, A., Dunn, C., Hale, M., Hutchins, G. & Treanor, D. The effect of quality control on accuracy of digital pathology image analysis. *IEEE Journal Of Biomedical And Health Informatics*. **25**, 307-314 (2020)
- [5] Hossain, M., Syeed, M., Fatema, K. & Uddin, M. The Perception of Health Professionals in Bangladesh toward the Digitalization of the Health Sector. *International Journal Of Environmental Research And Public Health*. **19**, 13695 (2022)
- [6] Pantanowitz, L., Szymas, J., Yagi, Y. & Wilbur, D. Whole slide imaging for educational purposes. *Journal Of Pathology Informatics*. **3**, 46 (2012)
- [7] Kumar, N., Gupta, R. & Gupta, S. Whole slide imaging (WSI) in pathology: current perspectives and future directions. *Journal Of Digital Imaging*. **33**, 1034-1040 (2020)
- [8] Hossain, M., Syeed, M., Fatema, K., Hossain, M. & Uddin, M. Singular Nuclei Segmentation for Automatic HER2 Quantification Using CISH Whole Slide Images. *Sensors*. **22**, 7361 (2022)
- [9] Rosenberg, A., Palmer, M., Merlino, L., Troost, J., Gasim, A., Bagnasco, S., Avila-Casado, C., Johnstone, D., Hodgins, J., Conway, C. & Others The application of digital pathology to improve accuracy in glomerular enumeration in renal biopsies. *PLoS One*. **11**, e0156441 (2016)
- [10] Mariani, L., Bomback, A., Canetta, P., Flessner, M., Helmuth, M., Hladunewich, M., Hogan, J., Kirylyuk, K., Nachman, P., Nast, C. & Others CureGN study rationale, design, and methods: establishing a large prospective observational study of glomerular disease. *American Journal Of Kidney Diseases*. **73**, 218-229 (2019)
- [11] Hossain, M., Hanna, M., Uraoka, N., Nakamura, T., Edelweiss, M., Brogi, E., Hameed, M., Yamaguchi, M., Ross, D. & Yagi, Y. Automatic quantification of HER2 gene amplification in invasive breast cancer from chromogenic in situ hybridization whole slide images. *Journal Of Medical Imaging*. **6**, 047501 (2019)
- [12] Shakhawat, H., Nakamura, T., Kimura, F., Yagi, Y. & Yamaguchi, M. Automatic Quality Evaluation of Whole Slide Images for the Practical Use of Whole Slide Imaging Scanner. *ITE Transactions On Media Technology And Applications*. **8**, 252-268 (2020)
- [13] Kanwal, N., Pérez-Bueno, F., Schmidt, A., Engan, K. & Molina, R. The Devil is in the Details: Whole Slide Image Acquisition and Processing for Artifacts Detection, Color Variation, and Data Augmentation: A Review. *IEEE Access*. **10** pp. 58821-58844 (2022)
- [14] Kothari, S., Phan, J. & Wang, M. Eliminating tissue-fold artifacts in histopathological whole-slide images for improved image-based prediction of cancer grade. *Journal Of Pathology Informatics*. **4**, 22 (2013)
- [15] Bautista, P. & Yagi, Y. Detection of tissue folds in whole slide images. 2009 Annual International Conference Of The IEEE Engineering In Medicine And Biology Society. pp. 3669-3672 (2009)
- [16] Kanwal, N., Fuster, S., Khoramnia, F., Zuiverloon, T., Rong, C. & Engan, K. Quantifying the effect of color processing on blood and damaged tissue detection in Whole Slide Images. 2022 IEEE 14th Image, Video, And Multidimensional Signal Processing Workshop (IVMSP). pp. 1-5 (2022)
- [17] Babaie, M. & Tizhoosh, H. Deep features for tissue-fold detection in histopathology images. *European Congress On Digital Pathology*. pp. 125-132 (2019)
- [18] Hossain, M., Nakamura, T., Kimura, F., Yagi, Y. & Yamaguchi, M. Practical image quality evaluation for whole slide imaging scanner. *Biomedical Imaging And Sensing Conference*. **10711** pp. 203-206 (2018)
- [19] Palokangas, S., Selinmaki, J. & Yli-Harja, O. Segmentation of folds in tissue section images. 2007 29th Annual International Conference Of The IEEE Engineering In Medicine And Biology Society. pp. 5641-5644 (2007)
- [20] Kothari, S., Phan, J., Stokes, T. & Wang, M. Pathology imaging informatics for quantitative analysis of whole-slide images. *Journal Of The American Medical Informatics Association*. **20**, 1099-1108 (2013)
- [21] Foucart, A., Debeir, O. & Decaestecker, C. Artifact identification in digital pathology from weak and noisy supervision with deep residual networks. 2018 4th International Conference On Cloud Computing Technologies And Applications (Cloudtech). pp. 1-6 (2018)
- [22] Janowczyk, A., Zuo, R., Gilmore, H., Feldman, M. & Madabhushi, A. HistoQC: an open-source quality control tool for digital pathology slides. *JCO Clinical Cancer Informatics*. **3** pp. 1-7 (2019)
- [23] Martel Assessment of Residual Breast Cancer Cellularity after Neoadjuvant Chemotherapy using Digital Pathology [Data set]. (<https://doi.org/10.7937/TCIA.2019.4YIBTJNO>)
- [24] Jha, D., Riegler, M., Johansen, D., Halvorsen, P. & Johansen, H. Doublet-net: A deep convolutional neural network for medical image segmentation. 2020 IEEE 33rd International Symposium On Computer-based Medical Systems (CBMS). pp. 558-564 (2020)
- [25] Ronneberger, O., Fischer, P. & Brox, T. U-net: Convolutional networks for biomedical image segmentation. *International Conference On Medical Image Computing And Computer-assisted Intervention*. pp. 234-241 (2015)

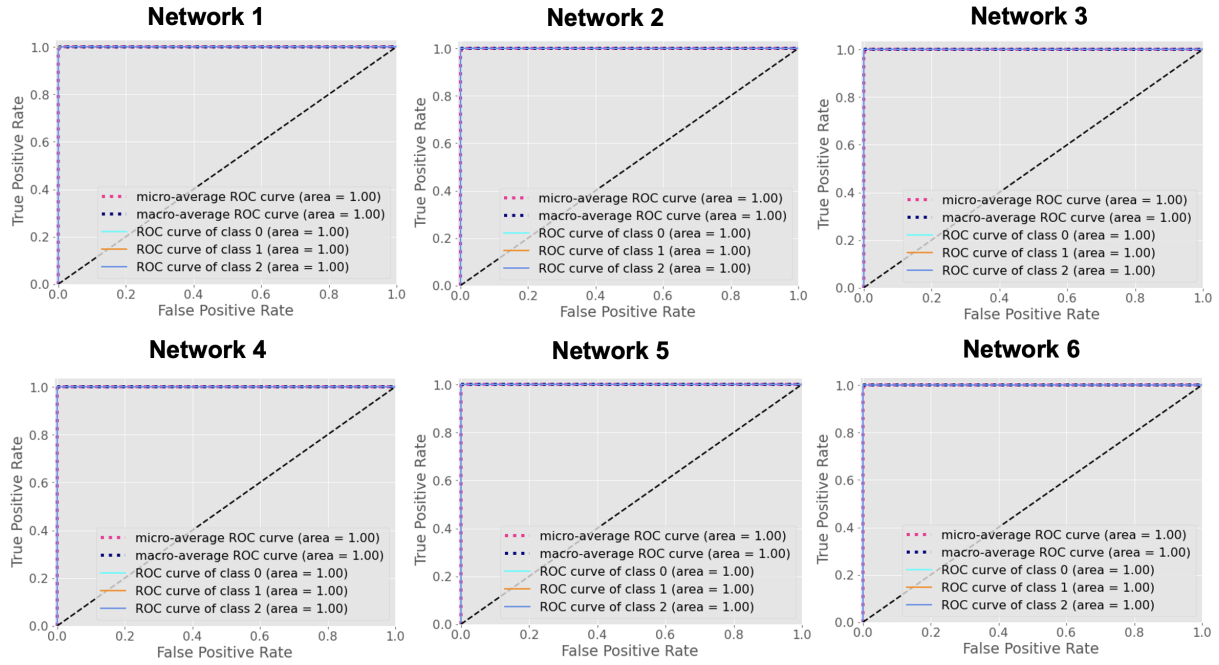


FIGURE 11. Receiver operating characteristic to multi-class for selected networks.

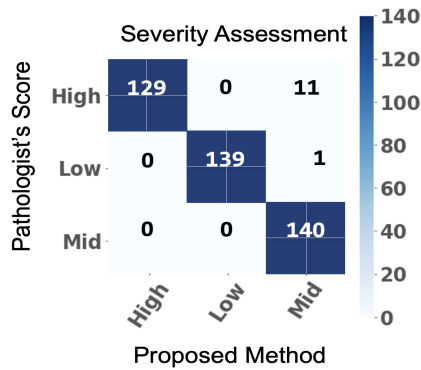


FIGURE 12. Comparison between proposed method and pathologist's manual score in terms of severity for test data.

- [26] Simonyan, K. & Zisserman, A. Very deep convolutional networks for large-scale image recognition. ArXiv Preprint ArXiv:1409.1556. (2014)
- [27] Mohammed, M., Mwambi, H., Mboya, I., Elbashir, M. & Omolo, B. A stacking ensemble deep learning approach to cancer type classification based on TCGA data. Scientific Reports. **11**, 1-22 (2021)
- [28] Su, R., Liu, X., Xiao, G. & Wei, L. Meta-GDBP: a high-level stacked regression model to improve anticancer drug response prediction. Briefings In Bioinformatics. **21**, 996-1005 (2020)
- [29] Hossain, M., Raihan, M., Hossain, M., Syeed, M., Rashid, H. & Reza, M. Aedes Larva Detection Using Ensemble Learning to Prevent Dengue Endemic. BioMedInformatics. **2**, 405-423 (2022)



HOSSAIN MD. SHAKHAWAT is an Assistant Professor in the Computer Science & Engineering Department of Independent University Bangladesh. His research focuses on using Machine Learning and Whole Slide Image Analysis techniques to gain insight into the treatment of cancer patients. He received his PhD degree from Tokyo Institute of Technology, Japan. Later worked as a Research Scientist in Memorial Sloan Kettering Cancer Center, USA. He also received an offer to join Oxford University, UK as a Senior Researcher of Machine Learning in Medical Imaging. Recently, his work is focused on unravelling the role of the HER2 (human epidermal growth factor receptor 2) gene in the growth of different cancers such as breast, colon and gastric. He is a member of the Association of Pathology Informatics, USA.



GALIB MUHAMMAD SHAHRIAR received M.Sc degree in Computer Science and Engineering from American International University-Bangladesh, Bangladesh. His research interest include Machine Learning, Computer Vision and Medical Image Analysis.



M MAHBUBUL SYEED received the Ph.D. degree. He is currently serving as an Associate Professor with the Department of CSE, IUB. He is the Project Coordinator for “Coding-for-All” Initiative, IUB, and the Deputy Director at the RIoT Research Center, IUB. He is also leading the OBE Curriculum Development Committee, CSE, IUB. In the recent past, he has completed his tenure as the Head of the Department of CS, AIUB. He has long track of teaching and research experience at

tertiary level. During the past 18 years, he served as a Distinguished Faculty and a Researcher in multiple renowned universities both in Bangladesh and abroad. His work experience includes, working at the Tampere University of Technology, Finland, as a Researcher and a Faculty, at the European Space Agency as a Senior Research Scientist, and as an Architect at Orange Telecom, France. His research work has produced 40 scholarly publications which are published in international ranked forums. During his research career, he achieved several research project fundings including three European research projects. His research interests include software engineering, software project development and management, the IoT/NB-IoT for intelligent system development, outcome based education (OBE) curriculum design, development and automation, and image processing. During his Ph.D. degree, he is awarded twice by Nokia Research Foundation for excellent research.



MD. SAKIR HOSSAIN (M'18) received his Ph.D. in Information and Computer Science from Saitama University, Saitama, Japan. Before obtaining his Ph.D., he had received his M.Sc. and B.Sc. in Information and Communication Engineering from University of Rajshahi, Bangladesh. He currently works as an Associate Professor at the Department of Computer Science, American International University-Bangladesh (AIUB), Bangladesh. In 2019, he worked as a postdoctoral

researcher at Czech Technical University, Prague, Czech Republic. As a postdoctoral researcher, he did research in interference management for unmanned aerial vehicle (UAV) assisted wireless networks. He works on development of solutions for networking and security with special focus on UAV-assisted wireless networks, intrusion detection systems, malware analysis, 6G wireless security, and Internet of things.



MOHAMMAD FAISAL UDDIN received the B.Sc. degree in electrical and electronics engineering from the Islamic University of Technology (IUT), Dhaka, Bangladesh, in 2002, and the M.A.Sc. and Ph.D. degrees in electrical and computer engineering from Concordia University, Montreal, QC, Canada, in 2006 and 2012, respectively. He is currently an Assistant Professor with the Department of Computer Science and Engineering, Independent University, Bangladesh

(IUB), Dhaka. He is also leading the RIoT Research Centre, IUB, as the Director. Before joining IUB in January 2018, he was working with Tata Communication Ltd., Matawan, NJ, USA, as a Principal Ethernet Engineer, where he worked on designing Ethernet networks. His research interest includes optimization theory and its applications.



RUBINA BARI received her Bachelor of Medicine, Bachelor of Surgery (MBBS) degree from Dhaka Medical College, Bangladesh. Later she has completed her Membership of the College of Bangladesh and Surgeons (MCPS) and Fellow of College of Physicians and Surgeons (FCPS in OBGYN and Pathology). Currently, she is a Consultant at Narayanganj Government Hospital of Bangladesh.



MAHADY HASAN received the bachelor's degree in computer science from Independent University, Bangladesh, in 2001, the master's degree in information technology from The University of Sydney, in 2004, and the Ph.D. degree in spatial database from the Computer Science and Engineering Department, University of New South Wales (UNSW), in 2010. Prior to joining IUB as an Assistant Professor, he served at UNSW, Australian Pacific College, and James Cook University, Australia. He has been working at IUB, since 2004. Currently, he is the Head of the Department of Computer Science and Engineering, as an Associate Professor. He is also the Director of FAB Laboratory and leading the industrial automation wing at the RIoT Center, IUB. He has published several book chapters, journals, and conference papers in many renowned venues. His research interests include software engineering, big data, data analytics, and engineering education.

...